This article has been accepted for publication in a future issue of this journal, but has not been fully edited. Content may change prior to final publication. Citation information: DOI 10.1109/TVT.2017.2664099, IEEE Transactions on Vehicular Technology

Multiple Frequency Band Channel Modeling and Analysis for Magnetic Induction Communication in Practical Underwater Environments

Hongzhi Guo, *Student Member, IEEE,* Zhi Sun, *Member, IEEE,*
and Pu Wang, *Member, IEEE*

***Abstract*—While underwater communications have been investigated for decades, existing solutions still have difficulties in establishing reliable and low-delay links among small-size devices. The Magnetic Induction (MI) communication is a promising solution due to its advantages in low propagation delay and less susceptibility to surrounding environments. To date, existing MI models cannot characterize broadband and complex underwater MI channels, especially in the shallow and lossy water, which significantly underestimates the underwater MI's performance. Moreover, the unpredictable polarization loss of coil antenna that makes MI unreliable has not been modeled and addressed. To this end, this paper presents a broadband channel model for underwater MI communication in complex environments. Compared with existing underwater MI models, the developed model can characterize: (i) the underwater magnetic field propagation at any point in the 3D space between the water surface and water floor, (ii) both the near and far fields of all feasible underwater signal bands; (iii) the impacts of lossy underwater medium on not only the propagation path but also the MI antenna itself; and (iv) the arbitrarily orientated Tri-directional (TD) coil antenna that can eliminate the MI antenna's susceptibility to orientation changes. The developed model is validated through COMSOL-Multiphysics simulations and in-lab experiments.**

***Index Terms*—Lateral wave, magnetic induction communication, tri-directional coil antenna, underwater communication.**

I. Introduction

Underwater wireless communication enables the real-time information sharing among networks of various underwater devices, such as underwater sensors and unmanned vehicles/robots [2]. Although the underwater wireless solutions have been investigated and implemented for decades long, existing techniques that are based on acoustic wave [3], optical wave [4], or Radio Frequency (RF) signal [5] still have difficulties in establishing reliable and low-latency wireless underwater links among small-size devices. In particular, RF signal experiences high attenuation in underwater environments, while optical waves suffer from scattering of light, both of which severely limit the achievable communication range and reliability. Meanwhile, acoustic waves, while promising long communication range in underwater, exhibit high propagation delay along with unreliable and unpredictable channel behavior, which is caused by complex multipath fading, prevalent Doppler effects, and significant variation of these properties due to temperature, salinity, or pressure [6].

Recently, the Magnetic Induction (MI) techniques have shown great potentials in wireless communications in RF-challenging environments, including underground [7] and underwater [6], [8]–[10]. Due to the unique advantages in low propagation delay and less susceptibility to the transmission environments, MI techniques become a promising solution to address the aforementioned challenges in underwater wireless communications. First, MI relies on the near field component of the magnetic field generated by coil antennas, which penetrates the lossy underwater medium much more efficiently than the far field EM waves. Second, the MI signal travels at the speed of 3×10^7 m/s in sea water, much faster than the acoustic waves. Hence, the propagation delay in MI is extremely small. Third, the impacts of multipath fading and scattering are minimized in the near field-based MI communications. As a result, the MI underwater channel is reliable and predictable.

The MI underwater channel model is essential to design and implement the underwater communication system as well as the whole networking protocol stack. However, it is challenging to accurately characterize the underwater MI channel, especially between the compact and mobile devices/robots in complex underwater environments, such as rivers and lakes. For example, the robotic fishes maneuver themselves as real fishes which can provide real-time underwater information [11], [12]. The communications between active robots require that the range can be as long as tens of meters and the wireless channel should be robust to their movement in 3D underwater environment. Despite the great efforts made in the existing related works [9], [10], [13], [14], the following four challenges in modeling the underwater MI channel have not been addressed.

- First, the impacts of practical underwater system and complex underwater environments need to be accurately characterized. However, the existing underwater MI models are based on some strict assumptions, such as huge wireless transceivers, expensive devices, infinitely large environments without boundaries, and idealized coil antenna.
- Second, all the frequency bands (including HF, MF, LF,

This work was supported by US National Science Foundation (NSF) under Grant CNS-1547908, CNS-1446484, and CNS-1446557. A shorter version of this paper was presented in [1].

Hongzhi Guo and Zhi Sun are with Department of Electrical Engineering, State University of New York at Buffalo, Buffalo, NY 14260. E-mail: {hongzhig, zhisun}@buffalo.edu. Pu Wang is with Department of Electrical Engineering & Computer Science, Wichita State University, Wichita, KS 67260. E-mail: pu.wang@wichita.edu

This article has been accepted for publication in a future issue of this journal, but has not been fully edited. Content may change prior to final publication. Citation information: DOI 10.1109/TVT.2017.2664099, IEEE Transactions on Vehicular Technology

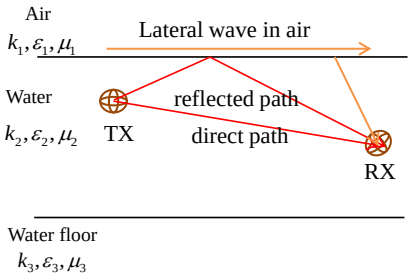

Fig. 1: Illustration of MI communication using Tri-directional (TD) coil antenna in underwater environment.

and VLF) that are possible for underwater communication need to be modeled. The existing underwater MI channel models work in HF band [9], [10] while most underwater EM field analysis focuses on LF or VLF bands. Those existing works need to be modified to model broader band due to their specific assumptions on the ratio of the signal wavelength to the transmission distances.

- Third, the unique interaction between the MI coil transceivers and the lossy underwater channel needs to be quantitatively modeled. Different from the conventional EM wave-based communications, the MI transmitter is closely coupled with the MI receiver as well as the transmission medium. The underwater medium not only determines the intensity of coupling between MI transceivers but also adds additional impedance to the MI transceivers. However, no existing MI models have captured the above unique interactions.
- Fourth, the mobility, especially the rotation, of the underwater sensors/robots needs to be taken into consideration, because it is almost impossible to fix the position and direction of the small devices in the fluidic underwater environments. Since the coil antenna is linearly polarized, if the receiving coil antenna's axis is perpendicular to the incident magnetic field it cannot receive any power. In contrast, if the coil's axis is parallel with the incident magnetic field, it can receive the maximum power. Therefore, the underwater MI is highly susceptible to device rotation, which has not been modeled by existing underwater MI channel models.

In this paper, we develop a comprehensive underwater channel model for MI communication systems, which can address the above four challenges. In particular, the developed model rigorously characterizes: (i) the underwater magnetic field propagation at any point in the 3D space between the water surface and water floor, (ii) both the near and far fields of all feasible underwater signal bands, including VLF, LF, MF, and HF bands; (iii) the impacts of lossy underwater medium (i.e., the water conductivity) on not only the propagation path but also the MI antenna itself; and (iv) the arbitrarily orientated Tri-directional (TD) coil antenna that can eliminate the MI antenna's susceptibility to orientation changes. The considered wireless channel and the MI system are illustrated in Fig. 1. The TD coil consists of three mutually perpendicular unidirectional (UD) coils. Each one of the three UD coils forms a beam along one of the three axes in the Cartesian coordinates. The three beams covers the entire 3D underwater space. As a result, no matter how the TD coil antenna rotates in the space, MI links can be reliably kept. In fact, although the TD coil antenna greatly enhances the reliability of underwater MI communication, modeling the TD coil antenna in the complex shallow water environment requires nontrivial effort. To derive the channel model in this paper, the magnetic field generated by coil antenna with unit current is first theoretically developed and then validated by Finite Element Method (FEM) simulations and in-lab experiments. After that, the arbitrarily orientated TD coil is modeled and its impedance in lossy water medium is quantitatively analyzed and validated. Next, a TD coil-enabled MIMO system is introduced and its channel capacity model is derived. Finally, we provide analytical channel performance evaluation in conjunction with numerical analysis to prove the reliability of TD coil and find the optimal operating frequency for MI underwater communication.

The rest of this paper is organized as follows. The related works are discussed in Section II. Section III presents the radiation model for coil antennas and introduces the lateral waves. Based on the field analysis, Section IV investigates the random orientation and the impedance of TD coil antennas in lossy water medium. After that the channel capacity is provided and discussed in Section V. Finally, we conclude this paper in Section VI.

II. Related Work

Wireless underwater communication using magnetic loop antenna or electric dipole has been extensively studied in [13]–[17]. In [13], the radiated field in air by an underwater horizontal coil operating at KHz band is investigated. In [15], a closed-form analytical model is developed for a vertical dipole in sea. In [14], the rough water surface is taken into account to model the field propagation in sea. More impressively, the experiments in [8] and [18] validate the feasibility of communication by using coil antenna operating at MHz band. Several tens of meters communication range can be achieved in sea water. Different from these pioneering works, we focus on the wireless communication performance, i.e., path loss and channel capacity, of broadband (from VLF to HF) small coil antennas (several centimeter in radius) with arbitrary orientation in underwater environment.

Recently, two of the most relevant works using MI communication in underwater environment were presented in [9] and [10]. First, in [9], the MI technique is compared comprehensively with acoustic signal and RF signal to justify its benefits, which is consistent with [18]. Furthermore, a path loss model is developed and numerically evaluated based on equivalent circuit model. In [10], a wireless MI network is designed and its performance is discussed. To overcome the impact of lossy sea water, the superconducting quantum interference devices are introduced. Different from these works, we pay attention to shallow water where the water surface and lateral wave cannot be ignored. In addition, we adopt smaller coil antennas and the impact of lossy medium on transceiver is modeled. Since our targeting application is underwater robots, we consider the antenna is arbitrarily orientated due to robot movement. To

This article has been accepted for publication in a future issue of this journal, but has not been fully edited. Content may change prior to final publication. Citation information: DOI 10.1109/TVT.2017.2664099, IEEE Transactions on Vehicular Technology

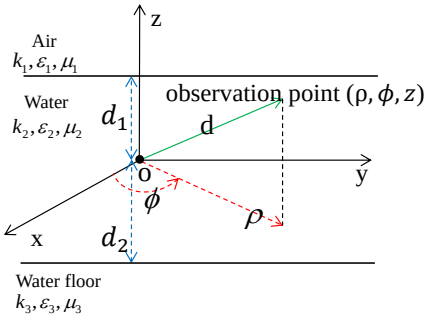

Fig. 2: Cylindrical coordinates of transceiver position. The transmitting TD coil is located at origin o.

alleviate the effect of antenna rotation, the TD coil is employed to increase the polarization diversity. The TD coil has been utilized for magnetic motion sensors [19] and wireless power transmission [20]. More relevantly, a modulation scheme is designed for TD coil in [21] to increase the channel capacity of magnetic induction communication for underground mine rescue. Since in underwater environment, the vertical antenna and horizontal antenna have drastically different performance and antenna rotation is frequent, the TD coil is a promising candidate to provide a robust channel. To sum up, in this paper, we take into account the antenna impedance, lateral wave, random antenna orientation, broad range of water conductivity and operating frequency, and channel capacity to develop a comprehensive MI underwater channel model.

III. Underwater Field Analysis for MI System

In this section, by considering a real MI coil antenna (excited by a unit current, i.e., 1 A), we derive the broadband (literally any frequency band) radiated field by determined orientated coils in practical underwater environments (with boundaries). After that, the field propagation mechanism in underwater environment is analyzed. The developed model in this section can be extended to arbitrarily orientated TD coil antenna model in next section.

In the rest of this paper, we use boldface lowercase letters for vectors and boldface capital letters for matrices. For a vector $\mathbf{h}_z$, h_z denotes its magnitude and $\hat{z}$ denotes its direction. For a matrix $\mathbf{T}$, $\mathbf{T}^T$ denotes its transpose, $\mathbf{T}^\dagger$ denotes its complex transpose and $\mathbf{T}^{-1}$ denotes its inverse.

A. Radiated Fields by Coil Antenna in Underwater

Before embarking on the analysis on radiated fields, the system coordinate is first provided in Fig. 2. There are three layers in the considered underwater environment, namely, air, water and water floor. The transmitting coil is located at origin o. The air-water interface is located at $z = d_1$ and the water-floor interface is at $z = -d_2$. The radial distance is denoted by ρ, which will be utilized to derive the lateral wave. The propagation constant, permeability, and permittivity are denoted by k, μ and ϵ, respectively. Note that $k = \omega\sqrt{\mu\epsilon}$ and $\epsilon = \epsilon_r + j\frac{\sigma}{\omega}$, where ϵ_r is the real part of the permittivity and σ is the conductivity of the medium. As shown in the figure, we use subscript 1, 2 and 3 to denote the corresponding dielectric parameters in air, water, and water floor, respectively.

The water surface and water floor are considered as flat in this paper due to the following two reasons. First, the communication range is within tens of meters and thus within such area the variance of water surface is not large. Second, since the frequency is from VLF to HF, the wavelength is long and the small roughness on the surface can be neglected [22], [23].

First, we consider three UD coil antennas whose orientations are along x, y, and z axis, respectively. Note that, with respect to the water-air interface, the $x-$ and $y-$orientated coil antennas are horizontal and $z-$orientated coil antenna is vertical. As illustrated in Fig. 1, the fields propagate in three ways: the direct path, reflected path, and lateral wave on the surface. Here we adopt the general EM model in layered medium [24], [25] to formulate the radiated magnetic fields by horizontal and vertical magnetic coil antenna:

$$\mathbf{h}^*_{cl}(\omega,\mathbf{d}) = \begin{bmatrix} h^*_\rho(\omega,\mathbf{d}) \\ h^*_\phi(\omega,\mathbf{d}) \\ h^*_z(\omega,\mathbf{d}) \end{bmatrix} = \int_{-\infty}^{\infty} \begin{bmatrix} \psi^*_1(k_\rho,\mathbf{d}) & \psi^*_1(k_\rho,\mathbf{d}) \\ \psi^*_3(k_\rho,\mathbf{d}) & \psi^*_3(k_\rho,\mathbf{d}) \\ 0 & 0 \end{bmatrix} \begin{bmatrix} \psi^*_2(k_\rho,\mathbf{d}) & -\psi^*_2(k_\rho,\mathbf{d}) \\ \psi^*_4(k_\rho,\mathbf{d}) & -\psi^*_4(k_\rho,\mathbf{d}) \\ \psi^*_5(k_\rho,\mathbf{d}) & \psi^*_5(k_\rho,\mathbf{d}) \end{bmatrix} \begin{bmatrix} \xi^*_1(k_\rho,\mathbf{d}) \\ \xi^*_2(k_\rho,\mathbf{d}) \\ \xi^*_3(k_\rho,\mathbf{d}) \\ \xi^*_4(k_\rho,\mathbf{d}) \end{bmatrix} dk_\rho \quad (1)$$

where $*$ denotes the $*$-orientated coil, i.e., x, y, and z, cl means the fields are expressed in cylindrical coordinates, $\mathbf{d}$ is a vector which points from the origin to the observation point, and ψ^*_i and ξ^*_i are determined by $*$ and its detailed expressions are provided in Appendix A.

B. Theoretical Analysis

Although (1) is a general solution with high accuracy, its integrand contains Hankel function and thus we can get limited theoretical insights from it. In this subsection, we theoretically analyze the field propagation mechanism of MI communication system in practical underwater environments, by some mathematical simplifications of (1). Plenty of efforts have been spent to obtain a succinct analytical model of lateral waves in stratified medium, such as underground and underwater [26]–[29]. However, all of these works consider electric antenna, or magnetic antenna with specific orientation which can not provide universal solutions to randomly orientated antennas. Here, we consider that both the transmitter and receiver are located in the water layer. In addition, since one of the challenges we plan to solve is the modeling in complex shallow water environment, we assume $d_1 < d_2$ and $d_1 << \rho$ in this subsection. It should be noted that this assumption is only for clearer theoretical insights. The complete field formulation in (1) can model any point in the 3D underwater space. By adopting the method in [15], [30], we can obtain the following equations which can provide insightful understanding of field propagation. The detailed deductions are relegated to Appendix B. For a z-orientated coil, the prominent magnetic fields can be expressed as

$$h^z_\rho(j\omega,\mathbf{d}) \approx \frac{jI_0Na^2k_1^2}{2k_2d^2} e^{j2k_2d_1 - jk_2z_r + jk_1d}; \quad (2a)$$

$$h^z_\phi(j\omega,\mathbf{d}) = 0; \quad (2b)$$

This article has been accepted for publication in a future issue of this journal, but has not been fully edited. Content may change prior to final publication. Citation information: DOI 10.1109/TVT.2017.2664099, IEEE Transactions on Vehicular Technology

$$h_z^z(j\omega, \mathbf{d}) \approx \frac{jI_0Na^2k_1^3}{2k_2^2d^2} e^{j2k_2d_1 - jk_2z_r + jk_1d}; \tag{2c}$$

where I_0 is the current in this z-orientated coil, a is coil radius, z_r is the observation point's z coordinate, N is the number of turns, and $d = \|\mathbf{d}\| \approx \rho$. As shown in (2), the field decays as distance d increases with the propagation constant of air k_1. Thus, even the antennas are in lossy water, the lateral waves propagate in the air along the water-air interface which decays much slower. In addition, the field propagates along the direct path and reflected path can be approximated by

$$\hat{h}_\rho^z(\omega, \mathbf{d}) = \frac{I_0Na^2k_2^2}{4d^2} e^{jk_2d}; \tag{3a}$$

$$\hat{h}_\phi^z(\omega, \mathbf{d}) = 0; \tag{3b}$$

$$\hat{h}_z^z(\omega, \mathbf{d}) = \frac{-I_0Na^2k_2}{4d} e^{jk_2d}. \tag{3c}$$

The detailed derivation is also provided in Appendix B. In view of (3), the field decays in speed of e^{jk_2d}. Since k_2 has a large imaginary part due to the conductivity of water, the fields attenuates much faster than lateral wave. In general, by taking a close look at (2) and (3), we can find that in the near region, especially when $d < 2d_1 - z_r$, the direct path is dominant since the fields lost more power when it propagates to the water-air interface; in the far region, i.e., $d >> d_1$, the lateral wave experiences less loss since it only propagates in water for a length $2d_1 - z_r$ and the rest of the path is in air. In contrast, the direct and reflected path propagate in water for d which suffer from high loss. Consequently, in order to achieve long distance communication in underwater environment (especially in sea water) by using magnetic field, lateral wave is a crucial component.

Besides the lateral wave, we also need to emphasize that antenna orientation can play an important role in both signal transmitting and receiving. Coil is a linear-polarized directional antenna. Specifically, if the receiving coil's axis is parallel with the incident magnetic field, it can collect the most power. Nevertheless, it cannot receive power if its axis is perpendicular to the magnetic field. Therefore, the orientation of a receiving coil is one of the most important factors which affect the performance of MI communication. Different from the receiving coil, the transmitting coil in the near field (smaller than one wavelength) is almost isotropic in free space since the difference between the maximum radiated field (polar angle is 0) and the minimum field (polar angle is 90) is 3 dB [31]. In other words, in free space, no matter how the transmitting coil antenna rotates, the change of magnetic field at the observation point in the near field should be no larger than 3 dB. Thus, the transmitting coil antenna as a radiator for near field communication is almost not directional. However, in underwater environment besides the receiving coil, the orientation of the transmitting coil can also dramatically affect the communication performance due to the inhomogeneous medium. Similar as the z-orientated coil, the magnetic fields radiated by the x- and y-orientated coil can be written as

$$h_\rho^{x/y}(\omega, \mathbf{d}) \approx \frac{-jI_{x/y}Na^2k_1}{2d^2} e^{j2k_2d_1 - jk_2z_r + jk_1d} \cos\phi_{x/y}; \tag{4a}$$

$$h_\phi^{x/y}(\omega, \mathbf{d}) \approx \frac{I_{x/y}Na^2}{2d^3} e^{j2k_2d_1 - jk_2z_r + jk_1d} \sin\phi_{x/y}; \tag{4b}$$

$$h_z^{x/y}(\omega, \mathbf{d}) \approx \frac{-jI_{x/y}Na^2k_1^2}{2k_2d^2} e^{j2k_2d_1 - jk_2z_r + jk_1d} \cos\phi_{x/y}. \tag{4c}$$

We can observe that $h_\rho^{x/y}(\omega, \mathbf{d})/h_\rho^z(\omega, \mathbf{d}) = k_2/k_1$ and $h_z^{x/y}(\omega, \mathbf{d})/h_z^z(\omega, \mathbf{d}) = k_2/k_1$ by neglecting the effect of azimuthal angle. Since $h_\rho^{x/y}(\omega, \mathbf{d})$ is much stronger than the other two components, we can claim that the magnetic field intensity generated by x/y-orientated coil is k_2/k_1 times larger than that generated by z-orientated coil. Consider that water has much larger permittivity and conductivity than air, k_2/k_1 is significant which means the horizontal coil antenna is more efficient than the vertical coil antenna. As a result, the orientation of the transmitting coil is as important as that of the receiving coil. This challenge also motivates us to introduce the TD coil.

C. Numerical Analysis

Based on the developed model, the effect of lateral wave and the vital importance of antenna orientation are demonstrated through numerical results and FEM simulation in COMSOL Multiphysics. Since MI communication is envisioned to enable applications which demand small antenna size, such as robotic fish and wireless sensors, we set the antenna radius as 5 cm and the number of turns is 5. The coil is provided with 1 A peak-to-peak current at frequency 10 MHz. The permittivity of the three layers are set as $\epsilon_{r1} = \epsilon_0$, $\epsilon_{r2} = 81\epsilon_0$, and $\epsilon_{r3} = 10\epsilon_0$, respectively. All of the three layers have the same permeability which is μ_0. Note that ϵ_0 and μ_0 are the permittivity and permeability of vacuum, respectively. The conductivity of the water and water floor are 0.1 S/m and 0.01 S/m, respectively. The geometry of the simulation model is depicted in Fig. 3a. A magnetic dipole antenna with current 1 A is located at the center of the simulation space and the middle layer is water with total depth 5 m. Also, observe that in Fig. 3b the magnetic field intensity changes dramatically on the water-air interface due to the large propagation constant in water.

There are mainly four factors that can significantly affect magnetic field, namely, depth, antenna orientation, operating frequency, and water conductivity. In Fig. 4a and Fig. 4b, the depth and antenna orientation effects are evaluated. The water conductivity σ_2 is set as 0.1 S/m. In Fig. 4a, the transmitting antenna's depth is 0.5 m and receiving antenna's depth are 0.2 m and 0.8 m. In Fig. 4b the transmitting antenna's depth is 2 m and the receiving antenna's depth are 1 m and 3 m. The magnetic field is calculated from transmitter to receiver and the distance is increased from 0.1 m to 15 m. The configurations are the same for analytical calculation and FEM simulation. The results further confirm the two primary conclusions we drew from the analytical discussions. First, the lateral wave only takes strong effect when the summation of transmitting antenna's and receiving antenna's depth is smaller than lateral distance. As shown in Fig. 4a and Fig. 4b, when distance is smaller than 3 m and 6 m, respectively, magnetic field attenuates exponentially due to the lossy water. Then, after that, it attenuates much slower thanks to the lossless propagation on the surface. Thus, the larger the depth, the

This article has been accepted for publication in a future issue of this journal, but has not been fully edited. Content may change prior to final publication. Citation information: DOI 10.1109/TVT.2017.2664099, IEEE Transactions on Vehicular Technology

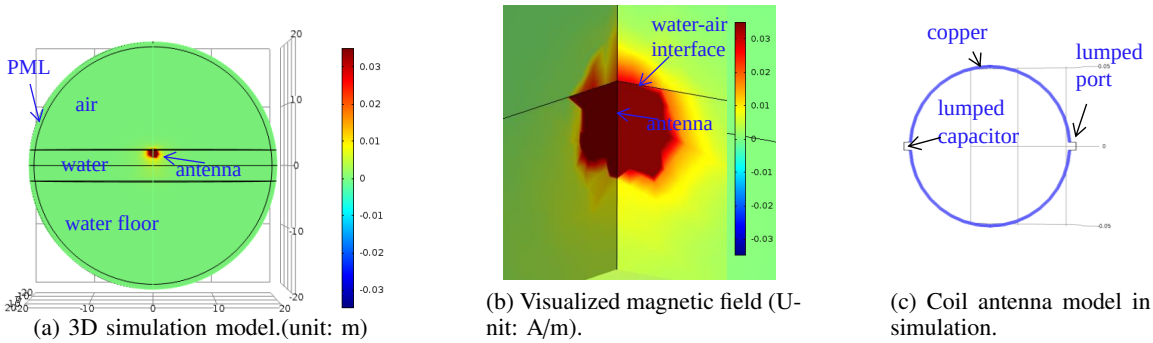

(a) 3D simulation model.(unit: m)

(b) Visualized magnetic field (Unit: A/m).

(c) Coil antenna model in simulation.

Fig. 3: Comsol simulation model and field intensity.

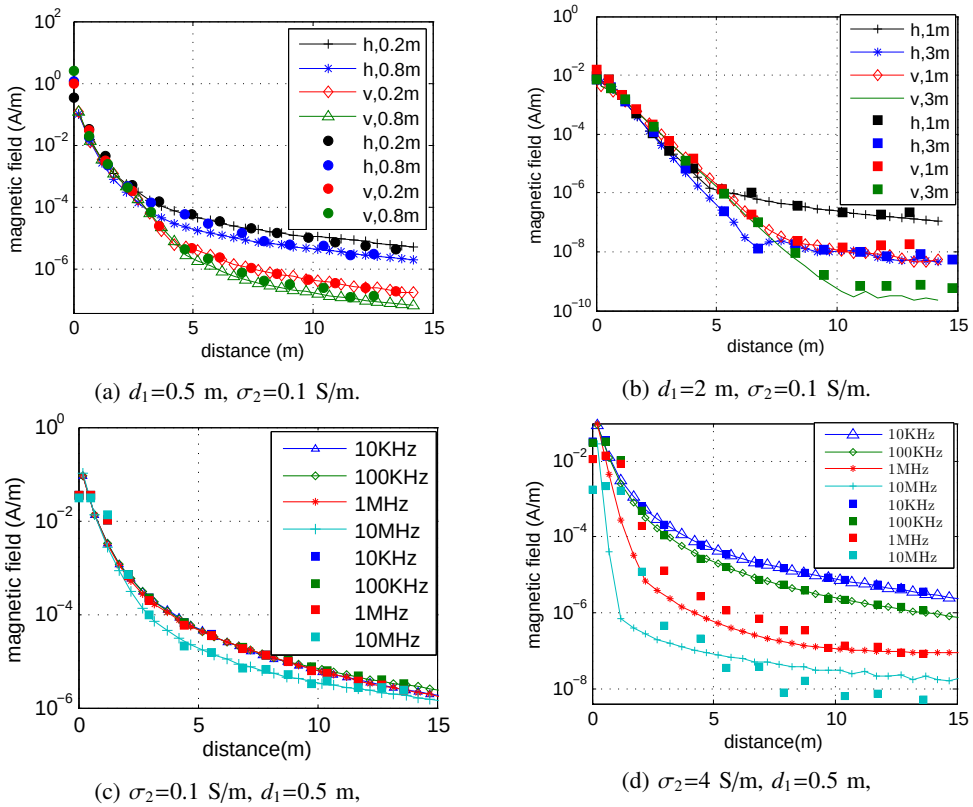

(a) d_1=0.5 m, σ_2=0.1 S/m.

(b) d_1=2 m, σ_2=0.1 S/m.

(c) σ_2=0.1 S/m, d_1=0.5 m,

(d) σ_2=4 S/m, d_1=0.5 m,

Fig. 4: Effects of receiving antenna depth, orientation, and operating frequency. v is vertical antenna and h is horizontal antenna. The lines with marker are analytical results and the colored markers without line are simulation results.

longer distance we need to see the effect of lateral wave. In addition, the effect of antenna orientation is investigated by setting the transmitting antenna to be z-orientated (vertical) and y-orientated (horizontal). The magnetic field generated by vertical antenna is around 10 dB smaller than that generated by horizontal antenna when distance is reasonably large. Referring back to (2) and (4), the dominant field is h_ρ and h_ρ^z is k_1/k_2 times smaller than h_ρ^y. Note that $\epsilon_2 = 81\epsilon_0 + j\sigma_2/\omega$ and $\epsilon_1 = \epsilon_0$. As a result, k_2 is a little more than 10 times larger than k_1 which leads to the difference. Next, we investigate the operating frequency and water conductivity. The transmitting antenna's depth is 0.5 m and observation point's depth is 0.2 m. The frequency is changed from 10 KHz to 10 MHz and the considered water conductivity is 0.1 S/m (lake water) and 4 S/m (sea water). As suggested in Fig. 4c and Fig. 4d, when conductivity is small, from 10 KHz to 10 MHz, magnetic fields have similar intensity. However, when the conductivity becomes dramatically large, the field intensity of 10 KHz is much larger than that of 10 MHz. When the water depth and conductivity are large, the deviation between analytical results and simulation results becomes large. This is due to the rapid oscillation of the integrand [24]. We use Gauss-Legendre quadrature to approximately calculate the field intensity and as the depth and conductivity increases more degrees are needed to maintain the accuracy. The primary reason of most existing works do not consider RF signal, especially in High Frequency (HF) band, in underwater environment is because of the significant attenuation which is demonstrated in Fig. 4d. However, this does not hold in lake water where conductivity is much smaller than sea water. With similar field intensity, HF can provide much larger bandwidth which is favorable for wireless communication. If the underwater

This article has been accepted for publication in a future issue of this journal, but has not been fully edited. Content may change prior to final publication. Citation information: DOI 10.1109/TVT.2017.2664099, IEEE Transactions on Vehicular Technology

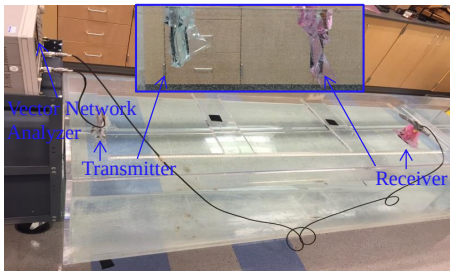

(a) Experiment setup.

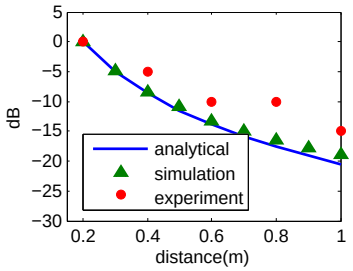

(b) Field intensity attenuation (S_{21} parameter).

Fig. 5: Experiment

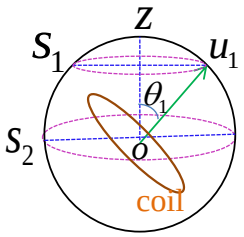

Fig. 6: Illustration of coil orientation.

conductivity further reduces, the HF band signal may achieve better performance. Consequently, the optimal frequency for MI underwater communication is highly influenced by the water conductivity and ranges from VLF, LF, MF, to HF band, which can be quantitatively determined based on our channel model.

D. In-lab Experiment Validation

In order to further validate the developed underwater MI model, an in-lab experiment was conducted. The result is compared with simulation and analytical results. As shown in Fig. 5a, two square coils with 10 cm side length and 8 turns are connected to the vector network analyzer. Since the coil size is much smaller than the wavelength, this square coil can also be regarded as a magnetic dipole which is the same as the circular coil. Meanwhile, a capacitor is in series with the coil to compensate the inductance. The operating frequency is set as 1 MHz and the coil is placed horizontally. Since the induced voltage in the receiving coil is proportional to magnetic field and the voltage at an observation point divided by the voltage at a reference point is proportional to S_{21} parameter [32], we measure the S_{21} parameter in experiment and simulation while we calculate the analytical magnetic field based on the developed model. Finally, the results are normalized by the value at the reference point to show the attenuation of magnetic field. In the simulation, we use the coil shown in Fig. 3c and only the transmitter's lumped port is excited to measure the S_{21} parameter. The lumped capacitor is also used to make the coil resonant at 1 MHz. Since the water in the tank has very low conductivity, in the analytical calculation and FEM simulation we consider the low conductivity, i.e., 0.01 S/m. The depth of the transmitter antenna is 10 cm and the receiver antenna is 15 cm. The interval between each measurement is 20 cm. As shown in Fig. 5b, the magnetic field intensities derived from the developed model, FEM simulation, and in-lab experiments match well with each other. However, there is several dB mismatch among them. The discrepancy is primarily due to the constrained environment in the tank, which generates stronger field intensity. The tank works as a waveguide to provide better propagation environment. However, in the numerical analysis and simulation, the medium is infinite. Therefore, the field intensity in experiment is higher than analytical and simulation results.

IV. Underwater Tri-directional Coil Antenna Model

Based on the field analysis in Section III, we investigate the influence of random orientated (instead of fixed) coil antenna with limited transmission power (instead of unit current) in this section. It should be noted that the field model derived in the previous section requires two conditions: unit exciting current and fixed orientation of the MI coil antenna. Those two conditions are relaxed in this section. We consider the TD coil antenna are three independent magnetic loop antennas with mutually perpendicular orientation. The modeling and experiments in [21] and [33] have proved the accuracy of this model.

A. Modeling the Random Coil Orientation

The transceivers' position is denoted in Cylindrical coordinates using (ρ, z, ϕ) and the orientation of a UD coil antenna on a transceiver is denoted denoted by a unit vector $\mathbf{u} = [u^x,\ u^y,\ u^z]$ as shown in Fig. 6. The end of the unit vector can be any point on the sphere shown in Fig. 6 and the way to find the direction of a vector with uniform distribution is provided in Appendix C. Once the orientation of an UD coil is found, the TD coil can be denoted by three unit vectors. In particular, the orientation of the transmitting coil and receiving coil can be expressed as

$$\mathbf{T} = \begin{bmatrix} t_1^x & t_1^y & t_1^z \\ t_2^x & t_2^y & t_2^z \\ t_3^x & t_3^y & t_3^z \end{bmatrix} \qquad \mathbf{R} = \begin{bmatrix} r_1^x & r_1^y & r_1^z \\ r_2^x & r_2^y & r_2^z \\ r_3^x & r_3^y & r_3^z \end{bmatrix}. \tag{5}$$

Moreover, as discussed before, the three vectors should be mutually perpendicular. Thus, $\mathbf{TT}^T = \mathbf{RR}^T = \mathbf{I}$, where $\mathbf{I}$ is an identity matrix. Note that $\mathbf{T}$ and $\mathbf{R}$ are orthogonal matrices. Without loss of generality, the first vector $\mathbf{t}_1$ can be generated by using the same way to create an UD coil, i.e., $P(\mathbf{t}_1)$ is the same as an UD coil. Then, $P(\mathbf{t}_2|\mathbf{t}_1) = \frac{1}{2\pi}$ since $\mathbf{t}_2$ should be located on the plane which is perpendicular to $\mathbf{t}_1$. In other words, we regard $\mathbf{t}_1$ as an axis and rotate $\mathbf{t}_2$, the end of $\mathbf{t}_2$ can only be located on a circle with circumference 2π. Once $\mathbf{t}_1$ and $\mathbf{t}_2$ are found, $\mathbf{t}_3$ should be determined. Hence, $P(\mathbf{t}_3|\mathbf{t}_1, \mathbf{t}_2) = 1$. Consequently, the random orientations of the transmitting coil antenna and receiving coil antenna are captured.

B. Field from Randomly Orientated Tri-directional Coil

For a randomly orientated TD coil in Fig. 7(a), the radius a and number of turns N are the same for the three UD coils C_1, C_2 and C_3. Since the antenna size is much smaller than

This article has been accepted for publication in a future issue of this journal, but has not been fully edited. Content may change prior to final publication. Citation information: DOI 10.1109/TVT.2017.2664099, IEEE Transactions on Vehicular Technology

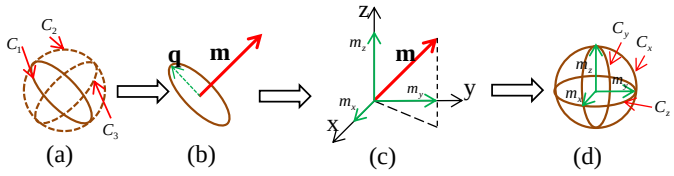

Fig. 7: Decomposition of magnetic dipole moment and equivalent TD coil.

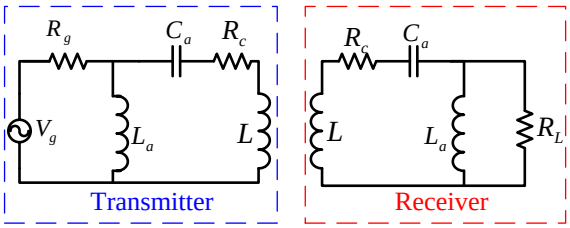

Fig. 8: Equivalent circuit of the coil antenna with impedance matching.

the wavelength, the coil antenna can be safely regarded as magnetic dipole. The dipole moment for each UD coil is $\mathbf{m}_l = m_l \cdot \mathbf{u}_l$, where $l = 1, 2, 3$, $m_l = \pi a^2 N I_l$, and $\mathbf{u}_l = [u_l^x,\ u_l^y,\ u_l^z]$. The dipole moment can be decomposed as $[m_l \cdot u_l^x,\ m_l \cdot u_l^y,\ m_l \cdot u_l^z]$. Then, we can add together the three dipole moments on the same direction. For instance, the dipole moment along x-axis can be written as

$$\mathbf{m}^x = [m_1 u_1^x + m_2 u_2^x + m_3 u_3^x, 0, 0]. \tag{6}$$

By using the same procedure, we can obtain $\mathbf{m}^y$, and $\mathbf{m}^z$. Consider the dipole moments $\mathbf{m}^x$, $\mathbf{m}^y$, and $\mathbf{m}^z$ relating to three equivalent UD coils which are perpendicular to each other, we formally substitute an arbitrarily orientated TD coil with three fixed UD coils whose axes are the same as the Cartesian coordination's axes as shown in Fig. 7(d). Substituting the corresponding dipole moments to the magnetic field expressions in (1), we can find the radiated field by $x-$, $y-$, and $z-$ orientated coil antenna which is equivalent to the field radiated by the TD coil antenna.

C. Influence of Water Medium on Antenna Impedance

Now we relax the assumption of fixed current in the transmitting coil. Instead, the fixed transmission power is utilized. As a result, the antenna impedance need to be considered. A unique impact of the lossy underwater medium on MI communication is to add additional coil impedance in the MI coupling.

As shown in Fig. 8, a UD coil's input impedance can be written as $Z_i = R_c + j\omega L$, where R_c is coil wire resistance and L is its self-inductance. The source resistance and load resistance are denoted by R_g and R_L. Such electrically small coil antenna has much smaller coil resistance than the typical R_g and R_L. Hence, the capacitor C_a and lumped inductor L_a are employed to form a L-network [34] to match the circuit. In this paper, since we consider a broad range of operating frequency, the wire's skin effect should be taken into account. Thus, R_c is a function of frequency. Moreover, since the coil is placed in lossy water medium, in the vicinity of the coil there is an additional ohmic loss. To model this additional loss, the self-inductance is considered as a complex number and its imaginary part is contributed by the additional loss.

1) Wire Resistance: Since the frequency range is broad, all those factors which can be affected by frequency should be treated carefully to avoid any misleading results. First, due to different skin depth of the wire at different frequencies, the AC resistance is more reasonable to describe the wire's resistance which is

$$R_c(\omega) = \frac{2aN}{\sigma_c \left[r_w^2 - \left(r_w - \sqrt{\frac{2}{\sigma_c \omega \mu_0}} \right)^2 \right]}, \tag{7}$$

where r_w is wire radius, and σ_c is the conductivity of the wire.

2) Self-inductance: Besides the loss in the wire, there is an additional loss in the vicinity of the coil caused by the lossy medium. In this paper, the self-inductance is modeled as a complex number to include both the inductance and the vicinity loss, i.e. $L = L_r - jL_i$, where L_r is the real part, L_i is the imaginary part, and both of them are real positive number. Since the impedance of an inductor is $Z_L = j\omega L = j\omega L_r + \omega L_i$, the imaginary part is actually the additional ohmic loss. Thus, an UD coil's resistance can be written as $R_c^t(\omega) = R_c(\omega) + \omega L_i$.

Due to the reflected field and lateral wave, underwater self-inductance of a coil is rather complicated. In the vicinity of the coil, the dominant field is the direct radiated field by the coil. Other reflected fields can be omitted since they are much weaker. Thus, the self-inductance of a coil can be expressed as

$$L = \frac{\Phi_0}{I_0} \approx \frac{N^2 \pi a \mu_2}{2} \left[\cos(k_{2r} a) - j \sin(k_{2r} a) \right] e^{-k_{2i} a}, \tag{8}$$

where Φ_0 is the magnetic flux through the coil, I_0 is coil's current, k_{2r} and k_{2i} are the real and imaginary part of k_2 respectively, which can be expressed as

$$\begin{aligned} k_{2r} &\approx 0.707\omega \sqrt{\mu_2 \epsilon_{r2}} \left\{ [1 + (\sigma_2/\omega\epsilon_{r2})^2]^{\frac{1}{2}} + 1 \right\}^{\frac{1}{2}}, \\ k_{2i} &\approx 0.707\omega \sqrt{\mu_2 \epsilon_{r2}} \left\{ [1 + (\sigma_2/\omega\epsilon_{r2})^2]^{\frac{1}{2}} - 1 \right\}^{\frac{1}{2}}. \end{aligned} \tag{9}$$

Equation (8) can be interpreted from two aspects. On one hand, when there is no conductivity, $k_{2r} = \omega \sqrt{\mu_2 \epsilon_{r2}}$ and $k_{2i} = 0$. Since for electrically small coil, $k_{2r} a$ is much smaller than 1. Accordingly, $\cos(k_{2r} a) \approx 1$ and $\sin(k_{2r} a) \approx 0$. Thus, the imaginary part of L can be neglected and the self-inductance in (8) is consistent with [7]. On the other hand, if there is high conductivity, k_{2r} increases and the imaginary part of L_c cannot be ignored. As a result, we can obtain a relatively large resistance.

In view of the developed model, the AC resistance is mainly affected by frequency and the external loss is determined by both frequency and water conductivity. In Fig. 9 we keep water conductivity as 0.1 S/m and investigate the frequency effect. When frequency is below 1 MHz, the resistance does not change too much and it is similar as DC resistance. However, when frequency is above 1 MHz, the resistance increases significantly. Meanwhile, the inductance is almost a constant. In Fig. 10, the frequency is kept as 10 MHz to investigate the effect of water conductivity. When water conductivity is larger than 0.001 S/m, the total resistance increases exponentially.

This article has been accepted for publication in a future issue of this journal, but has not been fully edited. Content may change prior to final publication. Citation information: DOI 10.1109/TVT.2017.2664099, IEEE Transactions on Vehicular Technology

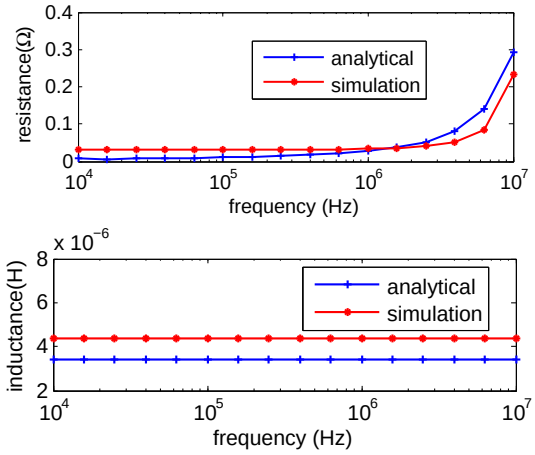

Fig. 9: Effect of frequency on resistance and self-inductance.

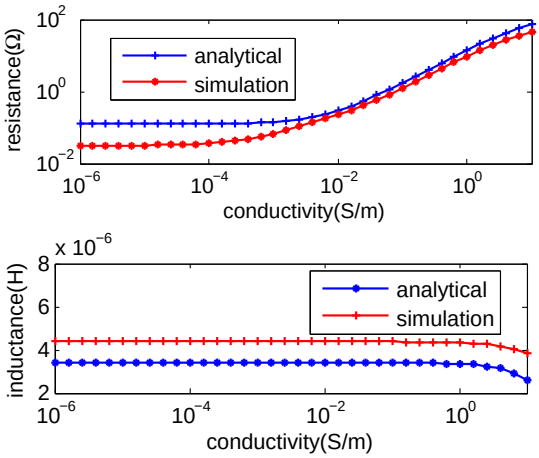

Fig. 10: Effect of water conductivity on resistance and self-inductance.

Also, the self-inductance deceases but much slower. Generally, both frequency and water conductivity can greatly influence antenna's impedance.

3) Power Transmission and Reception: Since the frequency and environment can significantly change the antenna's input impedance, a L-network is utilized to do impedance matching in order to make a fair comparison. Moreover, for the reason that the output impedance of the source is a constant 50 Ω and the coil input impedance varies with frequency, impedance matching is needed to let the coil antenna achieve its best performances. Let V_g denote the voltage provided by the generator and R_g stand for the output impedance. Then, the current in the antenna can be expressed as $I_0(\omega) = V_g(Z_1 \parallel Z_2)/[Z_1((Z_1 \parallel Z_2) + R_g)]$, where $Z_1 = R_c^t(\omega) + j\omega L + 1/(j\omega C_a)$, $Z_2 = j\omega L_a$, and $\parallel$ stands for parallel connection, for instance $Z_1 \parallel Z_2 = Z_1 Z_2/(Z_1 + Z_2)$. The value of the impedance matching inductor is $L_a = R_g\sqrt{R_c^t(\omega_0)}/[\omega_0\sqrt{R_g - R_c^t(\omega_0)}]$ and the capacitor is $C_a = 1/\left[\omega_0^2 L + \omega_0\sqrt{R_c^t(\omega_0)[R_g - R_c^t(\omega_0)]}\right]$. The transmission power is defined as the power delivered to the antenna which can be expressed as,

$$P_t(\omega) = \frac{1}{2}|I_0(\omega)|^2 \cdot R_c^t(\omega). \tag{10}$$

Here the real radiation resistance is not considered since the coil antenna's size is much smaller than the wavelength and MI communication does not rely on far field radiation. Notice that, (10) describes the transmission power for a single frequency. Assume that the bandwidth is $B_0 = f_h - f_l$, where f_l and f_h are the lower and upper frequency, respectively. The overall transmission power allocated in the bandwidth is $P_t^o = \frac{1}{2\pi}\int_{2\pi f_l}^{2\pi f_h} P_t(\omega)d\omega$. In view of (10), the transmission power is affected by frequency due to the mismatch when the frequency is shifted from ω_0. However, in fact, MI communication has very narrow bandwidth due to the intrinsic resonance. Thus, we can assume that within the bandwidth, P_t is a constant, i.e., $P_t^o = B_0 P_t(\omega_0)$.

Analogous to the transmitting coil, the receiving coil also has an impedance matching unit. The induced voltage in the receiving coil is denoted by $V_r(\omega)$ and the received power is

$$P_r(\omega) = \frac{1}{2R_L} \cdot \frac{V_r(\omega) \cdot V_r'(\omega) \cdot (Z_2 \parallel R_L) \cdot (Z_2 \parallel R_L)'}{(Z_1 + Z_2 \parallel R_L) \cdot (Z_1 + Z_2 \parallel R_L)'} \tag{11}$$

$$= \Gamma_r(\omega) \cdot |V_r(\omega)|^2. \tag{12}$$

From (11) we can see the received power is determined by $V_r(\omega)$. As have been discussed, $V_r(\omega)$ is proportional to magnetic field intensity which was derived in last section. Thus, it is served as a connection between the field analysis and equivalent circuit analysis. In next section, we derive $V_r(\omega)$ analytically, upon which the channel capacity can be obtained.

V. Channel Model and Characteristics Analysis

In this section, we complete the underwater MI channel model by integrating the formulations and analysis derived in the previous sections, which quantitatively capture the influence of coil antenna orientation, water conductivity, depth, operating frequency, and coil antenna input impedance. Then the channel model is used to analyze the underwater MI channel capacity and the reliability of TD coil antenna as well as the optimal operating frequency in different underwater environments.

A. Complete Channel Model

For a TD coil antenna, the power constraint is $\sum_{q=1}^{3} P_{tq}^o = P_t^o$, where P_{tq}^o is the power allocated to the q^{th} UD coil antenna. Then, we can find the power density is $P_{tq}(\omega) = P_{tq}^o/B_0$ and the current in an UD coil $I_q(\omega) = \sqrt{\frac{2P_{tq}(\omega)}{R_c^t(\omega)}}$. To make the deductions succinct, we use a dipole moment matrix

$$\mathbf{M}_{moment} = \begin{bmatrix} m_1 & 0 & 0 \\ 0 & m_2 & 0 \\ 0 & 0 & m_3 \end{bmatrix}. \tag{13}$$

where $m_x = I_x(\omega)\pi a^2 N, x = 1, 2, 3$. As a result, the magnetic field at the observation point can be written as

$$\mathbf{H}_t(\omega, \mathbf{d}) = \frac{1}{\pi a^2 N}\mathbf{H}_{cl}(\omega, \mathbf{d})(\mathbf{M}_{moment} \cdot \mathbf{T})^T, \tag{14}$$

where $\mathbf{H}_{cl}(\omega, \mathbf{d}) = [\mathbf{h}_{cl}^x(\omega, \mathbf{d}), \mathbf{h}_{cl}^y(\omega, \mathbf{d}), \mathbf{h}_{cl}^z(\omega, \mathbf{d})]$. Note that $\mathbf{H}_{cl}(\omega, \mathbf{d})$ is the field solution in Section III where the coil has unit current. Next, we convert the field from cylindrical coordinates to Cartesian coordinates by using the following

This article has been accepted for publication in a future issue of this journal, but has not been fully edited. Content may change prior to final publication. Citation information: DOI 10.1109/TVT.2017.2664099, IEEE Transactions on Vehicular Technology

relation

$$\begin{bmatrix} h_x(\omega,\mathbf{d}) \\ h_y(\omega,\mathbf{d}) \\ h_z(\omega,\mathbf{d}) \end{bmatrix} = \begin{bmatrix} \cos\phi & -\sin\phi & 0 \\ \sin\phi & \cos\phi & 0 \\ 0 & 0 & 1 \end{bmatrix} \cdot \begin{bmatrix} h_\rho(\omega,\mathbf{d}) \\ h_\phi(\omega,\mathbf{d}) \\ h_z(\omega,\mathbf{d}) \end{bmatrix} \quad (15)$$

$$= \mathbf{L}_t \cdot \mathbf{h}_{cl}(\omega,\mathbf{d}) \quad (16)$$

Matrix $\mathbf{L}_t$ transforms the magnetic field expressed in cylindrical coordinates to Cartesian coordinates to calculate the coil's received power. Then, based on the magnetic field, the mutual inductance between the transmitting TD coil and receiving TD coil can be written as

$$\mathcal{M} = \mathbf{\Phi}_r \mathbf{I}_c^{-1} = \mu_0 \pi a^2 N \mathbf{R} \mathbf{L}_t \mathbf{H}_{cl}(\omega,\mathbf{d}) \mathbf{T}^T, \quad (17)$$

where the elements in $\mathbf{\Phi}_r$ denotes the magnetic flux in each receiving coil generated by the transmitting UD coils. Here, $\mathcal{M}$ is a 3 by 3 matrix which contains the mutual inductance between the three transmitting UD coils and the three receiving UD coils. In the equivalent circuit we do not consider the impedance brought by mutual inductance due to the loose coupling which makes its value much smaller than the coil impedance without coupling. Finally, based on the mutual inductance, the induced voltage in the receiving TD coil can be obtained,

$$\mathbf{V}_r(\omega) = j\omega \mathcal{M} \mathbf{I}_c. \quad (18)$$

where $\mathbf{V}_r(\omega)$ is a 3 by 3 matrix and its elements $V_r^{m,n}(\omega)$ means the voltage in m^{th} receiving coil induced by the n^{th} transmitting coil.

Then, the channel capacity can be written as,

$$C = \frac{1}{2\pi} \int_{2\pi f_l}^{2\pi f_h} \log_2 \det \left[\mathbf{I} + \frac{\Gamma_r(\omega) \mathbf{V}_r(\omega) \mathbf{V}_r(\omega)^\dagger}{\mathcal{N}(\omega)} \right] d\omega \quad (19)$$

$$\approx B_0 \log_2 \det \left[\mathbf{I} + \frac{\Gamma_r(\omega_0) \mathbf{V}_r(\omega_0) \mathbf{V}_r(\omega_0)^\dagger}{\mathcal{N}(\omega_0)} \right] \quad (20)$$

$$\approx \sum_{q=1}^{3} B_0 \log_2 \left[1 + \frac{2\omega_0^2 \Gamma_r(\omega_0) P_{tq}(\omega_0) \lambda_q^2(\omega_0)}{R_c^t(\omega_0) \mathcal{N}(\omega_0)} \right], \quad (21)$$

where $\mathcal{N}(\omega)$ is the noise density, and $\lambda_q^2(\omega_0)$ is the eigenvalue of $\mathcal{M}\mathcal{M}^\dagger$. To approximate (19), in (20) we assume the transmission power density and noise power density are constant within the bandwidth B_0. Based on the developed channel capacity model, the reliability of tri-directional coil antenna and the optimal frequency in underwater environment are discussed qualitatively and quantitatively in the following.

B. Enhancing Reliability by TD Coil Antenna

The motivation of using TD coil antenna is to mitigate the impacts of the random orientation of the original UD coil antenna when the wireless devices rotate in water. From (17) to (21), we can see the difference between TD coil and UD coil on channel capacity. When both the transmitting and receiving antenna are UD coils, matrices $\mathbf{R}$ and $\mathbf{T}$ would be substituted by unit vectors $\mathbf{r}$ and $\mathbf{t}$, respectively. Thus, (18) can be updated as $v_r(\omega) = j\omega\mu_0\pi a^2 N I_0(\omega) \mathbf{r} \mathbf{L}_t \mathbf{H}_{cl}(\omega,\mathbf{d}) \mathbf{t}^T$. When $\mathbf{r} \cdot [\mathbf{L}_t \mathbf{H}_{cl}(\omega,\mathbf{d}) \mathbf{t}^T] = 0$, we cannot receive any information. In contrast, when $\mathbf{r}/\|\mathbf{r}\| = \pm[\mathbf{L}_t \mathbf{H}_{cl}(\omega,\mathbf{d}) \mathbf{t}^T]/\|\mathbf{L}_t \mathbf{H}_{cl}(\omega,\mathbf{d}) \mathbf{t}^T\|$, the receiver can collect the maximum power. Hence, UD coil antenna is highly unreliable. However, the envisioned underwater wireless devices are mobile, their antenna's orientations are not fixed.

The experiments in [33] prove the reliability of TD coil antenna. However, the existing works consider neither the transmitter nor receiver has the Channel State Information (CSI) which underestimates its performance. In this paper, we explore more advantages of the TD coil antenna and rigorously and theoretically prove the reliability of TD coil antenna. Specifically, we proceed to the scenario where the receiver has access to the CSI or both of the transmitter and receiver have CSI. In the former scenario the transmission power is equally allocated to the three UD coils, while in the later the transmission power is allocated based on waterfilling algorithm [35].

Referring back to (21), the capacity of TD coil is directly related to the eigenvalues of $\mathcal{M}\mathcal{M}^\dagger$. Although the rotation of the TD coil antennas can generate random matrices $\mathbf{R}$ and $\mathbf{T}$, the summation of the eigenvalues of $\mathcal{M}\mathcal{M}^\dagger$ are not influenced by the rotation. By using (18), we can obtain

$$\mathcal{M}\mathcal{M}^\dagger = \mu_0^2 \pi^2 a^4 N^2 \mathbf{R} \mathbf{L}_t \mathbf{H}_{cl}(\omega,\mathbf{d}) \mathbf{T}^T \mathbf{T} \mathbf{H}_{cl}^\dagger(\omega,\mathbf{d}) \mathbf{L}_t^T \mathbf{R}^T. \quad (22)$$

Since $\mathbf{R}$ and $\mathbf{T}$ are orthogonal matrices, $\mathcal{M}\mathcal{M}^\dagger$ is a similar matrix of

$$\widetilde{\mathbf{W}} = \mu_0^2 \pi^2 a^4 N^2 \mathbf{L}_t \mathbf{H}_{cl}(\omega,\mathbf{d}) \mathbf{H}_{cl}^\dagger(\omega,\mathbf{d}) \mathbf{L}_t^T. \quad (23)$$

$\mathcal{M}\mathcal{M}^\dagger$ and $\widetilde{\mathbf{W}}$ share the same eigenvalues. More importantly, we find that $\widetilde{\mathbf{W}}$ is independent of antenna orientation. Therefore, by using TD coil with CSI we can eliminate the effect of UD coil's random orientation and, ultimately, a stable wireless channel can be formed. Furthermore, if we can pick up the best pair of transmitting UD coil and receiving UD coil, the best channel can always be formed no matter how the device rotates. This can be done by using waterfilling. In the following we assume the CSI is available at the transmitter.

Next, we numerically evaluate the channel capacity of randomly orientated TD coil and UD coil. Three scenarios are considered which are UD coil transceivers, TD coil transceivers with equal power allocation, and TD coil transceivers with power waterfilling. The operating frequency is set as 10 MHz. The transmission power density is set as -10 dBm/Hz and the signal is corrupted by the thermal noise with power density -174 dBm/Hz [36], [37]. The numerical results are demonstrated in Fig. 11 where we plot the mean value, in conjunction with the maximum value and minimum value to show the reliability of TD coil.

First, we consider low water conductivity with σ_2=0.1 S/m. The transmitting and receiving antenna's depth in Fig. 11a and Fig. 11b are set as 0.5 m and 0.2 m, and 2 m and 1 m, respectively. Since the orientation is randomly generated, UD coil has a large fluctuation in channel capacity which demonstrates its unreliability. When the antennas are well aligned, the best capacity can be achieved. In contrast, as predicted by the analytical model, no matter what's TD coil's orientation, the channel capacity is always the same. Moreover, we notice that by using waterfilling, the capacity is similar as that without it. The reason is that here we consider a relatively low noise power density and the signal-to-noise ratio

This article has been accepted for publication in a future issue of this journal, but has not been fully edited. Content may change prior to final publication. Citation information: DOI 10.1109/TVT.2017.2664099, IEEE Transactions on Vehicular Technology

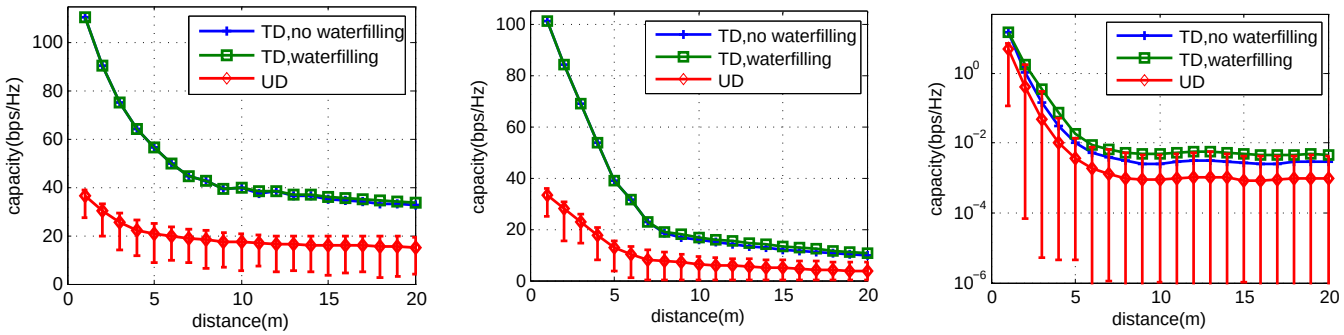

(a) TX:0.5 m; RX:0.2 m; σ_2:0.1 S/m (b) TX:2 m; RX:1 m; σ_2:0.1 S/m (c) TX:0.5 m; RX:0.2 m; σ_2:4 S/m

Fig. 11: Effect of antenna orientation on channel capacity.

(SNR) is high. As a result, the optimal strategy is allocate the power almost equally to the three UD coils in the TD coil. Consequently, there is no obvious difference.

Then, we consider water conductivity is much higher, i.e., 4 S/m, and SNR becomes low due to the high attenuation of magnetic field. As shown in Fig. 11c, channel capacity is dramatically reduced and the minimum channel capacity of UD coil is extremely small. In addition, due to the low SNR, we see a clear gap between TD coil with and without waterfilling. Although the TD coil without waterfilling has a stable channel, it still cannot achieve the largest channel capacity of UD coil. More impressively, the TD coil with waterfilling can achieve the upper bound channel capacity of optimally orientated UD coil. Intuitively, we pick up the best orientated UD coil in the TD coil and provide it with the full amount of power, then it behaves like the optimally orientated UD coil.

C. Optimal Frequency

The developed channel model reveals that both the coil antenna and propagation channel are susceptible to frequency change. On one hand, the low frequency is almost immune to high conductivity due to the long wavelength, while high frequency has very small skin depth in water which leads to significant loss. The additional antenna impedance brought by the lossy medium is also much more significant when high frequency band is used. As a result, most of existing works adopt low frequency for underwater communication. On the other hand, high frequency can provide strong coupling between MI coil antennas as well as broader bandwidth which is essential for wireless communication. Motivated by this, we re-exam the optimal frequency for underwater MI communication by using channel capacity as a metric.

Due to the intrinsic resonance of the coil antenna, it has maximum efficiency at the resonant frequency. However, since the impedance matching is designed at this single frequency, if the operating frequency deviates from resonant frequency there would be a mismatch between antenna and source which makes the antenna inefficient. As a result, the bandwidth of the antenna is very small. In [31], the bandwidth of an antenna is defined as a frequency range where a specific antenna parameter conforms to a standard. Here we use the received power in (10) which considers both antenna and channel as a standard to evaluate the bandwidth. If the operating frequency deviates from resonant frequency, there would be a mismatch between antenna and source which makes the antenna inefficient. Through increasing the frequency from $0.8\omega_0$ to $1.2\omega_0$, we find the upper and lower frequency where the ratio is 0.5 by which we can find the bandwidth. Once we have the bandwidth, by using (21) and waterfilling, the optimal channel capacity can be found. As shown in Fig. 12a, with 10 dBm transmission power when water conductivity is small, i.e., 0.1 S/m, 10 MHz performs much better due to the large bandwidth and similar field intensity as lower frequency. However, here we do not aggressively further increase the frequency since this would take antenna's AC resistance and channel propagation loss to a much higher level which can significantly deteriorate the performance. As depicted in Fig. 12b the capacity of 10 MHz decays fast as the depth increases. In Fig. 12c, when water conductivity increases to 4 S/m, 100 kHz performs better in the far region and 1 MHz performs better in near region both of which are much better than 10 MHz. In this scenario, the propagation loss is significant. Also, in view of Fig. 10, the resistance at 10 MHz with 4 S/m water conductivity is also large which dissipates much more power. Therefore, when water conductivity is high, such as sea water, 10 MHz is not preferred.

VI. Conclusion

In underwater communications, the Magnetic Induction (MI) technique shows unique advantages in reliability and low-latency over conventional technologies that are based on optical waves, acoustic waves, and RF signals. In this paper, an accurate and comprehensive channel model is developed for underwater MI system. Different from existing MI underwater channel models, the effect of lateral waves in shallow water region is quantitatively characterized. Moreover, the antenna model under the influences of lossy water medium is considered. The Tri-directional (TD) coil is utilized to against the unpredictable antenna orientation. Finally, the channel capacity is derived and the reliability and optimal frequency of the TD coil antenna-enabled MI underwater communication is discussed. The developed channel model is verified by finite element simulations. Through the modeling and analysis, we observe that the communication range of a MI system using small-size antennas (5 cm in radius) can be more than 20 m in underwater

This article has been accepted for publication in a future issue of this journal, but has not been fully edited. Content may change prior to final publication. Citation information: DOI 10.1109/TVT.2017.2664099, IEEE Transactions on Vehicular Technology

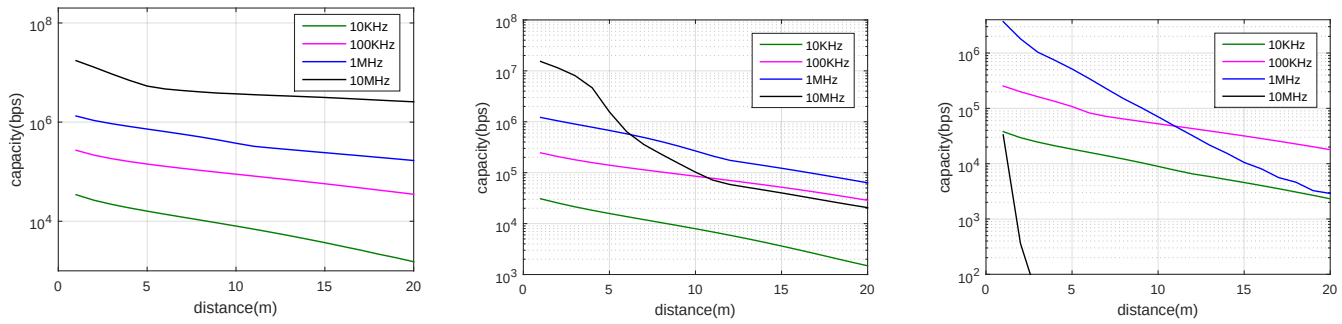

(a) TX, 0.5 m;RX, 0.2 m;σ_2=0.1 S/m (b) TX, 2 m; RX, 1 m;σ_2=0.1 S/m (c) TX, 0.5 m;RX, 0.2 m; σ_2=4 S/m

Fig. 12: Effect of operating frequency on channel capacity.

environment. Also, with the channel state information, the MI system is immune to the random orientation of coil antenna. The designed MI system is envisioned to enable the wireless communications among tiny wireless sensors and unmanned robots in underwater environment.

Appendix A
Expressions for Field Components in (1)

For z-orientated ($*=z$) coil,

$$\psi_1^z(k_\rho,\mathbf{d})=\psi_3^z(k_\rho,\mathbf{d})=\psi_4^z(k_\rho,\mathbf{d})=0; \tag{24a}$$

$$\psi_2^z(k_\rho,\mathbf{d})=\frac{-jk_{2z}}{k_\rho}H_1^{(1)}(k_\rho\rho); \tag{24b}$$

$$\psi_5^z(k_\rho,\mathbf{d})=H_0^{(1)}(k_\rho\rho); \tag{24c}$$

where $H_n^{(1)}$ is the n^{th} order of the first kind of Hankel function and k_ρ and k_z denote the propagation constant along ρ and z direction. For x-orientated ($*=x$) coil,

$$\psi_1^x(k_\rho,\mathbf{d})=\frac{-j\omega\epsilon_2}{k_\rho^2\rho}H_1^{(1)}(k_\rho\rho)\cos\phi_x; \tag{25a}$$

$$\psi_2^x(k_\rho,\mathbf{d})=\frac{jk_{2z}}{k_\rho}\left[\frac{H_1^{(1)}(k_\rho\rho)}{k_\rho\rho}-H_2^{(1)}(k_\rho\rho)\right]\cos\phi_x; \tag{25b}$$

$$\psi_3^x(k_\rho,\mathbf{d})=\frac{j\omega\epsilon_l}{k_\rho}\left[\frac{H_1^{(1)}(k_\rho\rho)}{k_\rho\rho}-H_2^{(1)}(k_\rho\rho)\right]\sin\phi_x; \tag{25c}$$

$$\psi_4^x(k_\rho,\mathbf{d})=\frac{-jk_{lz}}{k_\rho^2\rho}H_1^{(1)}(k_\rho\rho)\sin\phi_x; \tag{25d}$$

$$\psi_5^x(k_\rho,\mathbf{d})=H_1^{(1)}(k_\rho\rho)\cos\phi_x; \tag{25e}$$

Substituting ϕ_x in eqs. (25a) to (25e) with $\phi_x-\frac{\pi}{2}$, we can obtain the radiated field by y-orientated ($*=y$) coil.

For z-orientated ($*=z$) coil in water when $z>0$,

$$\xi_1(k_\rho,\mathbf{d})=\xi_2(k_\rho,\mathbf{d})=0, \tag{26a}$$

$$\xi_3(k_\rho,\mathbf{d})=\xi_4(k_\rho,\mathbf{d})/(\mathcal{R}_2e^{-j2k_{2z}z})=(1+\mathcal{R}_1)\gamma_1e^{jk_{2z}z}; \tag{26b}$$

for z-orientated ($*=z$) coil in water when $z<0$,

$$\xi_1(k_\rho,\mathbf{d})=\xi_2(k_\rho,\mathbf{d})=0, \tag{27a}$$

$$\xi_3(k_\rho,\mathbf{d})=\xi_4(k_\rho,\mathbf{d})\mathcal{R}_1/e^{-j2k_{2z}z}=\mathcal{R}_1(1+\mathcal{R}_2)\gamma_1e^{jk_{2z}z}; \tag{27b}$$

for x-orientated ($*=x$) and y-orientated ($*=y$) coil in water when $z>0$,

$$\xi_1(k_\rho,\mathbf{d})=\xi_2(k_\rho,\mathbf{d})/(\mathcal{R}_4e^{-j2k_{2z}z})=(1+\mathcal{R}_3)\gamma_2e^{jk_{2z}z}, \tag{28a}$$

$$\xi_3(k_\rho,\mathbf{d})=\xi_4(k_\rho,\mathbf{d})/(\mathcal{R}_2e^{-j2k_{2z}z})=(1-\mathcal{R}_1)\gamma_3e^{jk_{2z}z}; \tag{28b}$$

for x-orientated ($*=x$) and y-orientated ($*=y$) coil in water when $z<0$,

$$\xi_1(k_\rho,\mathbf{d})=\xi_2(k_\rho,\mathbf{d})\mathcal{R}_3/e^{-j2k_{2z}z}=\mathcal{R}_3(1+\mathcal{R}_4)\gamma_2e^{jk_{2z}z}, \tag{29a}$$

$$\xi_3(k_\rho,\mathbf{d})=\xi_4(k_\rho,\mathbf{d})\mathcal{R}_1/e^{-j2k_{2z}z}=-\mathcal{R}_1(1-\mathcal{R}_2)\gamma_3e^{jk_{2z}z}, \tag{29b}$$

where

$$\mathcal{R}_1=\frac{k_{2z}/k_{3z}-\mu_2/\mu_3}{k_{2z}/k_{3z}+\mu_2/\mu_3}e^{-j2k_{2z}d_2}; \tag{30a}$$

$$\mathcal{R}_2=\frac{k_{2z}/k_{1z}-\mu_2/\mu_1}{k_{2z}/k_{1z}+\mu_2/\mu_1}e^{j2k_{2z}d_1}; \tag{30b}$$

$$\mathcal{R}_3=\frac{k_{2z}/k_{3z}-\epsilon_2/\epsilon_3}{k_{2z}/k_{3z}+\epsilon_2/\epsilon_3}e^{-j2k_{2z}d_2}; \tag{30c}$$

$$\mathcal{R}_4=\frac{k_{2z}/k_{1z}-\epsilon_2/\epsilon_1}{k_{2z}/k_{1z}+\epsilon_2/\epsilon_1}e^{j2k_{2z}d_1}; \tag{30d}$$

$$\gamma_1=\frac{-jI_0Na^2k_\rho^3}{8k_{2z}(1-\mathcal{R}_1\mathcal{R}_2)};\gamma_2=\frac{I_0Na^2\omega\mu_2k_\rho^2}{8k_{2z}(1-\mathcal{R}_3\mathcal{R}_4)};\gamma_3=\frac{-I_0Na^2k_\rho^2}{8(1-\mathcal{R}_1\mathcal{R}_2)}. \tag{31}$$

Here I_0 should be consistent with the current in the corresponding coil.

Appendix B
Derivation of (2), (3) and (4)

By assuming that $d_1<<d_2$, $d_1<<d$, and $d_1>z_r>0$, we can obtain the following approximated equations. First, since water is lossy and k_2 has a large imaginary part, (30) can be simplified as follows,

$$\mathcal{R}_1=\mathcal{R}_3=0; \tag{32a}$$

$$\mathcal{R}_2\approx-e^{-2k_{1z}/k_{2z}+j2k_{2z}d_1}; \tag{32b}$$

$$\mathcal{R}_4\approx-e^{-2k_{2z}\epsilon_1/(k_{1z}\epsilon_2)+j2k_{2z}d_1}; \tag{32c}$$

Note that, the approximations in (32) is based on the Taylor series that $\ln(\frac{1+x}{1-x})\approx2x+2/3x^3$, when $-1<x<1$. Then, (31) can be updated as

$$\gamma_1\approx\frac{-jI_0Na^2k_\rho^3}{8k_{2z}};\quad\gamma_2\approx\frac{I_0Na^2\omega\mu_2k_\rho^2}{8k_{2z}};\quad\gamma_3\approx\frac{-I_0Na^2k_\rho^2}{8}; \tag{33}$$

We use h_ρ^z as an example to show how to simplify the integral based on the method in [15], [30]. Other magnetic fields can be found in the same way. According to (1),

$$h_\rho^z=\int_{-\infty}^{\infty}\left[\psi_2^z(k_\rho,\mathbf{d})\xi_3^z(k_\rho,\mathbf{d})-\psi_2^z(k_\rho,\mathbf{d})\xi_4^z(k_\rho,\mathbf{d})\right]dk_\rho. \tag{34}$$

Then, we divide h_ρ^z into f_1 and f_2 to solve them separately. By using the Sommerfeld Identity

$$\frac{2e^{jkd}}{jd} = \int_{-\infty}^{\infty} \frac{k_\rho}{k_z} H_0^{(1)}(k_\rho \rho) e^{jk|z|} dk_\rho. \tag{35}$$

we can obtain

$$\begin{aligned} f_1 &= \int_{-\infty}^{\infty} \psi_2^z(k_\rho, \mathbf{d}) \xi_3^{l_2,z}(k_\rho, \mathbf{d}) dk_\rho \\ &= \int_{-\infty}^{\infty} \left[\frac{-I_0 N a^2 k_\rho k_{2z}}{8} \frac{H_1^{(1)}(k_\rho \rho)}{H_0^{(1)}(k_\rho \rho)} \right] \left[\frac{k_\rho}{k_{2z}} H_0^{(1)}(k_\rho \rho) e^{jk_{2z} z_r} \right] dk_\rho \\ &\approx \frac{-I_0 N a^2 k_{\rho_0} \sqrt{k_2^2 - k_{\rho_0}^2}}{8} \frac{H_1^{(1)}(k_{\rho_0} \rho)}{H_0^{(1)}(k_{\rho_0} \rho)} \int_{-\infty}^{\infty} \frac{k_\rho}{k_{2z}} H_0^{(1)}(k_\rho \rho) e^{jk_{2z} z_r} dk_\rho. \end{aligned} \tag{36}$$

Next, according to (35) and (24) and (25) in [30], we can find the stationary phase point is $k_{\rho_0} = k_2 \sqrt{\frac{\rho^2}{\rho^2 + z_r^2}}$. Then, by substituting k_{ρ_0} into (36), we can obtain f_1 which is $\hat{h}_\rho^{l_2,z}(j\omega, \mathbf{d})$ in (3). Similarly,

$$\begin{aligned} f_2 &= -\int_{-\infty}^{\infty} \psi_2^z(k_\rho, \mathbf{d}) \xi_4^{l_2,z}(k_\rho, \mathbf{d}) dk_\rho = \int_{-\infty}^{\infty} \left[\frac{k_\rho}{k_{1z}} H_0^{(1)}(k_\rho \rho) e^{k_{1z} \frac{-2}{k_{2z}}} \right] \\ &\times \frac{-I_0 N a^2 k_\rho k_{1z}}{8} \frac{H_1^{(1)}(k_\rho \rho)}{H_0^{(1)}(k_\rho \rho)} e^{j2k_{2z} d_1 - jk_{2z} z_r} dk_\rho \\ &= \left[\frac{-I_0 N a^2 k_{\rho_0} \sqrt{k_1^2 - k_{\rho_0}^2}}{8} \frac{H_1^{(1)}(k_{\rho_0} \rho)}{H_0^{(1)}(k_{\rho_0} \rho)} e^{j2\sqrt{k_2^2 - k_{\rho_0}^2} d_1 - j\sqrt{k_2^2 - k_{\rho_0}^2} z_r} \right] \\ &\times \int_{-\infty}^{\infty} \left[\frac{k_\rho}{k_{1z}} H_0^{(1)}(k_\rho \rho) e^{k_{1z} \frac{-2}{k_{2z}}} \right] dk_\rho \end{aligned} \tag{37}$$

Finally, we can find f_2 by using the same method, which is $h_\rho^z(j\omega, \mathbf{d})$ and provided in (2).

Appendix C
Randomly Orientated Coil

Consider that there is a virtual sphere with radius 1 and origin o. The coil orientation is an unit vector $\mathbf{u}$ starting from the sphere's origin o and ending at a point u_1 on the sphere as shown in Fig. 6. Since the orientation is random, u_1 should be uniformly distributed on the sphere. The polar angle θ and azimuthal angle ϕ are utilized to denote the position. Since θ and ϕ are independent, the probability of a point u_1 located at (θ, ϕ) can be expressed as $P(\theta, \phi) = P(\theta)P(\phi)$.

We now divide the sphere into slices with infinitely small thickness and each slice is perpendicular to z-axis, such as slices s_1 and s_2 in Fig. 6. The probability of u_1 distributed on a slice is proportional to the circumference of that slice, i.e., $2\pi \sin\theta$. Then, $P(\theta)$ and its CDF (cumulative distribution function) can be expressed as

$$P(\theta) = \frac{1}{2} \sin\theta; \quad \Phi(\theta) = \frac{1}{2} - \frac{1}{2} \cos\theta. \tag{38}$$

The CDF function can be utilized to generate θ. For each slice, the point u_1 is distributed uniformly on the circle from $\phi = 0$ to $\phi = 2\pi$ with $P(\phi) = \frac{1}{2\pi}$. Then, $P(\theta, \phi) = \frac{1}{4\pi} \sin\theta$. By using the relation between Spherical coordinates and Cartesian coordinates, the expression of $\mathbf{u}$ can be found.

References

[1] H. Guo, Z. Sun, and P. Wang, "Channel modeling of mi underwater communication using tri-directional coil antenna," in *IEEE Globecom 2015*, San Diego, USA, Dec 2015.

[2] I. Akyildiz, D. Pompili, and T. Melodia, "Underwater acoustic sensor networks: Research challenges," *Elsevier's Journal of Ad Hoc Networks*, vol. 3, no. 3, pp. 257–279, 2005.

[3] M. Stojanovic and J. Preisig, "Underwater acoustic communication channels: Propagation models and statistical characterization," *Communications Magazine, IEEE*, vol. 47, no. 1, pp. 84–89, 2009.

[4] S. Jaruwatanadilok, "Underwater wireless optical communication channel modeling and performance evaluation using vector radiative transfer theory," *Selected Areas in Communications, IEEE Journal on*, vol. 26, no. 9, pp. 1620–1627, 2008.

[5] X. Che, I. Wells, G. Dickers, P. Kear, and X. Gong, "Re-evaluation of rf electromagnetic communication in underwater sensor networks," *Communications Magazine, IEEE*, vol. 48, no. 12, pp. 143–151, 2010.

[6] I. F. Akyildiz, P. Wang, and Z. Sun, "Realizing underwater communication through magnetic induction," *IEEE Communications Magazine*, vol. 53, no. 11, pp. 42–48, November 2015.

[7] Z. Sun and I. F. Akyildiz, "Magnetic induction communications for wireless underground sensor networks," *IEEE Transactions on Antenna and Propagation*, vol. 58, no. 7, pp. 2426–2435, July 2010.

[8] A. Al-Shamma'a, A. Shaw, and S. Saman, "Propagation of electromagnetic waves at mhz frequencies through seawater," *Antennas and Propagation, IEEE Transactions on*, vol. 52, no. 11, pp. 2843–2849, Nov 2004.

[9] M. C. Domingo, "Magnetic induction for underwater wireless communication networks," *IEEE Transactions on Antennas and Propagation*, vol. 60, no. 6, pp. 2929–2939, 2012.

[10] B. Gulbahar and O. B. Akan, "A communicatiion theoretical modeling and analysis of underwater magneto-inductive wireless channels," *IEEE Transactions on Wirelss Communications*, vol. 11, no. 9, pp. 3326–3334, 2012.

[11] X. Tan, "Autonomous robotic fish as mobile sensor platforms: Challenges and potential solutions," *Marine Technology Society Journal*, vol. 45, no. 4, pp. 31–40, 2011.

[12] D. Shin, S. Y. Na, J. Y. Kim, and S.-J. Baek, "Fish robots for water pollution monitoring using ubiquitous sensor networks with sonar localization," in *Convergence Information Technology, 2007. International Conference on*. IEEE, 2007, pp. 1298–1303.

[13] H. Wang, K. Zheng, K. Yang, and Y. Ma, "Electromagnetic field in air produced by a horizontal magnetic dipole immersed in sea: Theoretical analysis and experimental results," *Antennas and Propagation, IEEE Transactions on*, vol. 62, no. 9, pp. 4647–4655, 2014.

[14] O. M. Abo-Seida, S. T. Bishay, and K. M. El-Morabie, "Far-field radiated from a vertical magnetic dipole in the sea with a rough upper surface," *Geoscience and Remote Sensing, IEEE Transactions on*, vol. 44, no. 8, pp. 2135–2142, 2006.

[15] Y. Long, H. Jiang, and B. Rembold, "Far-region electromagnetic radiation with a vertical magnetic dipole in sea," *IEEE Transactions on antennas and propagation*, vol. 49, no. 6, pp. 992–996, 2001.

[16] R. W. King, "Electromagnetic field of a vertical dipole over an imperfectly conducting half-space," *Radio Science*, vol. 25, no. 2, pp. 149–160, 1990.

[17] R. W. King and M. F. Brown, "Lateral electromagnetic waves along plane boundaries: A summarizing approach," *Proceedings of the IEEE*, vol. 72, no. 5, pp. 595–611, 1984.

[18] C. Uribe and W. Grote, "Radio communication model for underwater wsn," in *2009 3rd International Conference on New Technologies, Mobility and Security*. IEEE, 2009, pp. 1–5.

[19] R. Zhu and Z. Zhou, "A real-time articulated human motion tracking using tri-axis inertial/magnetic sensors package," *IEEE Transactions on Neural systems and rehabilitation engineering*, vol. 12, no. 2, pp. 295–302, 2004.

[20] W. M. Ng, C. Zhang, D. Lin, and S. R. Hui, "Two-and three-dimensional omnidirectional wireless power transfer," *IEEE Transactions on Power Electronics*, vol. 29, no. 9, pp. 4470–4474, 2014.

[21] A. Markham and N. Trigoni, "Magneto-inductive networked rescue system (miners) taking sensor networks underground," in *IPSN 2012*, Beijing, China, April 2012.

[22] L. Tsang, J. Kong, and K. Ding, *Scattering of Electromagnetic Waves, Theories and Applications*, ser. A Wiley interscience publication. Wiley, 2000.

[23] T. S. Rappaport *et al.*, *Wireless communications: principles and practice*. prentice hall PTR New Jersey, 1996, vol. 2.

[24] W. Chew, *Waves and fields in inhomogeneous media*. Van Nostrand Reinhold, 1990.
[25] J. Kong, *Electromagnetic Wave Theory*, ser. A Wiley-interscience publication. Wiley, 1990.
[26] X. Dong and M. C. Vuran, "A channel model for wireless underground sensor networks using lateral waves," in *Global Telecommunications Conference (GLOBECOM 2011), 2011 IEEE*. IEEE, 2011, pp. 1–6.
[27] R. E. Collin, "Hertzian dipole radiating over a lossy earth or sea: some early and late 20th-century controversies," *IEEE Antennas and Propagation Magazine*, vol. 46, no. 2, pp. 64–79, 2004.
[28] T. Wu and R. King, "Lateral waves: A new formula and interference patterns," *Radio Science*, vol. 17, no. 3, pp. 521–531, 1982.
[29] R. Gabillard, P. Degauque, and J. Wait, "Subsurface electromagnetic telecommunication-a review," *IEEE Transactions on Communication Technology*, vol. 19, no. 6, pp. 1217–1228, 1971.
[30] W. Chew, "A quick way to approximate a sommerfeld-weyl-type integral," *Antennas and Propagation, IEEE Transactions on*, vol. 36, no. 11, pp. 1654–1657, 1988.
[31] C. A. Balanis, *Antenna Theory*. John Wiley Publishing Company, 2005.
[32] Y. Luo, Y. Yang, and Z. Chen, "Self-tuning wireless power transmission scheme based on on-line scattering parameters measurement and two-side power matching," *Scientific reports*, vol. 4, 2014.
[33] X. Tan, Z. Sun, and I. F. Akyildiz, "Wireless underground sensor networks: Mi-based communication systems for underground applications." *Antennas and Propagation Magazine, IEEE*, vol. 57, no. 4, pp. 74–87, 2015.
[34] D. M. Pozar, *Microwave engineering*. John Wiley & Sons, 2009.
[35] D. Tse and P. Viswanath, *Fundamentals of wireless communication*. Cambridge university press, 2005.
[36] J. B. Johnson, "Thermal agitation of electricity in conductors," *Physical review*, vol. 32, no. 1, p. 97, 1928.
[37] H. Nyquist, "Thermal agitation of electric charge in conductors," *Physical review*, vol. 32, no. 1, p. 110, 1928.

Hongzhi Guo (S'12) received his B.S. degree in Automation from Shandong University of Science and Technology, Qingdao, China, in 2011 and M.S. degree in Electrical Engineering from Columbia University, New York, NY, in 2013. Currently, he is a Ph.D. student in the Electrical Engineering Department at State University of New York at Buffalo, under guidance of Prof. Zhi Sun. His current research interests are in wireless system design in underground and underwater, metamaterial antenna design, wireless nano-biosensing, and signal detection and estimation.

Zhi Sun (M'11) received the B.S. degree in telecommunication engineering from Beijing University of Posts and Telecommunications (BUPT), Beijing, China, the M.S. degree in electronic engineering from Tsinghua University, Beijing, China, in 2004 and 2007, respectively, and the Ph.D. degree in electrical and computer engineering from Georgia Institute of Technology, Atlanta, GA, USA, in 2011. Currently, he is an Assistant Professor with the Department of Electrical Engineering, State University of New York at Buffalo, Buffalo, NY, USA. Prior to that, he was a Postdoctoral Fellow with Georgia Institute of Technology, Atlanta, GA, USA. Prof. Sun was the recipient of the Best Paper Award in the 2010 IEEE Global Communications Conference (Globecom). He was also the recipient of the BWN Researcher of the Year Award at Georgia Institute of Technology in 2009, and the Outstanding Graduate Award at Tsinghua University in 2007. His research interests include wireless communication and networking in complex environments, metamaterial enhanced communication and security, wireless intra-body networks, wireless underground networks, wireless underwater networks, and cyber physical systems.

Pu Wang (M'05) received the B.S. degree in Electrical Engineering from the Beijing Institute of Technology, Beijing, China, in 2003 and the M.Eng. degree in Computer Engineering from the Memorial University of Newfoundland, St. Johns, NL, Canada, in 2008. He received the Ph.D. degree in Electrical and Computer Engineering from the Georgia Institute of Technology, Atlanta, GA, in 2013. He is currently an Assistant Professor with the Department of Electrical Engineering and Computer Science, Wichita State University, Wichita, KS. He was named BWN Lab Researcher of the Year 2012, Georgia Institute of Technology. He received the TPC top ranked paper award of IEEE DySPAN 2011. He was also named Fellow of the School of Graduate Studies, 2008, Memorial University of Newfoundland. He is a member of IEEE. His research interests include wireless sensor networks, cognitive radio networks, software defined networks, nanonetworks, Internet of Things, and cyber-physical systems.